

# Topological Defects Induced High-Spin Quartet State in Truxene-Based Molecular Graphenoids

Can Li<sup>1\*</sup>, Yu Liu<sup>1†</sup>, Yufeng Liu<sup>1†</sup>, Fu-Hua Xue<sup>2</sup>, Dandan Guan<sup>1,3,4</sup>, Yaoyi Li<sup>1,3,4</sup>, Hao Zheng<sup>1,3,4</sup>, Canhua Liu<sup>1,3,4</sup>, Jinfeng Jia<sup>1,3,4</sup>, Pei-Nian Liu<sup>2</sup>, Deng-Yuan Li<sup>2\*</sup> & Shiyong Wang<sup>1,3,4\*</sup>

<sup>1</sup>Key Laboratory of Artificial Structures and Quantum Control, Ministry of Education, Shenyang National Laboratory for Materials Science, School of Physics and Astronomy, Shanghai Jiao Tong University, Shanghai 200240, <sup>2</sup>Key Laboratory for Advanced Materials and Feringa Nobel Prize Scientist Joint Research Center, Frontiers Science Center for Microbiology and Dynamic Chemistry, School of Chemistry and Molecular Engineering, East China University of Science and Technology, Shanghai 200237, <sup>3</sup>Tsung-Dao Lee Institute, Shanghai Jiao Tong University, Shanghai 200240, <sup>4</sup>Shanghai Research Center for Quantum Sciences, Shanghai 201315

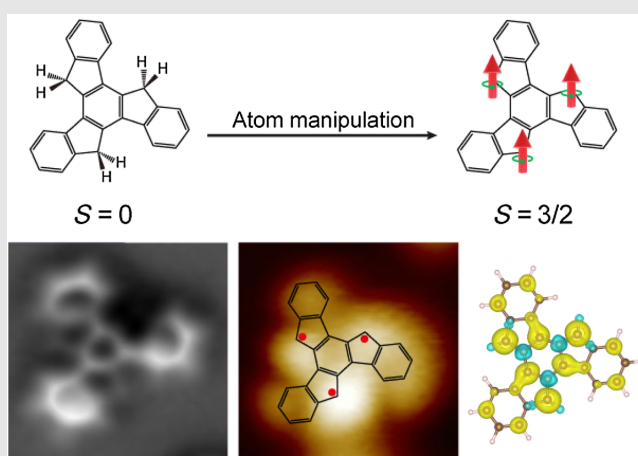
\*Corresponding authors: [lic\\_18@sjtu.edu.cn](mailto:lic_18@sjtu.edu.cn); [dengyuanli@ecust.edu.cn](mailto:dengyuanli@ecust.edu.cn); [shiyong.wang@sjtu.edu.cn](mailto:shiyong.wang@sjtu.edu.cn); <sup>†</sup>C. Li, Y. Liu, and Y. Liu contributed equally to this work.

Cite this: *CCS Chem.* **2023**, 5, 695–703

DOI: 10.31635/ccschem.022.202201895

Topological defects in graphene materials introduce exotic properties with both fundamental importance and technological implications, absent in their defect-free counterparts. Although individual topological defects have been widely studied, collective magnetic behaviors originating from well-organized multiple topological defects remain a great challenge. Here, we examined the collective magnetic properties originating from three pentagon topological defects in truxene-based molecular graphenoids using scanning tunneling microscopy (STM) and non-contact atomic force microscopy. Unpaired  $\pi$  electrons were introduced into the aromatic topology of truxene molecular graphenoids one by one by dissociating hydrogen atoms at the pentagon defects via atom manipulation. STM measurements, together with density functional theory calculations, suggested that the unpaired electrons were ferromagnetically coupled, forming a collective high-spin quartet state of  $S = 3/2$ . Our work demonstrates that collective spin ordering could be realized

through engineering regular patterned topological defects in molecular graphenoids, providing a new platform for designing one-dimensional ferromagnetic spin chains and two-dimensional ferromagnetic networks.



Keywords:  $\pi$  electron magnetism, STM/nc-AFM, high-spin molecules, atom manipulation, surface chemistry

## Introduction

Topological defects widely exist in graphene materials and locally change their intrinsic physical and chemical properties. Examples include  $sp^3$  carbons, vacancies, carbon tetragons, pentagons, heptagons, dislocations, and grain boundaries, which introduce intriguing electronic, magnetic, optical, and mechanical properties with implications for sensors, and electronics, spintronics, and quantum technologies.<sup>1-13</sup> Topological defects usually break the sublattice symmetry of graphene and introduce unconventional  $\pi$ -electron magnetism, with properties that differ from  $d/f$  electron magnetism.<sup>14</sup> In the past decade, intense research efforts have been devoted to studying such unconventional magnetism in graphene materials. Although many graphene systems exhibit signatures of the presence of  $sp^2$  carbon magnetism, it remains elusive to reveal collective magnetic behaviors originating from regular patterned topological defects. This is mainly because the topological defects are usually randomly interspersed in graphene lattice, and arranging these defects in a controllable way remains challenging using traditional top-down methods. Additionally, as the magnetism of graphene-based materials depends crucially on their atomic structure and surrounding environments, it requires the ability to fabricate samples with atomic precision and techniques to characterize them down to the single-chemical-bond level.

Recently, atomically precise segments of graphene, also named nanographenes or molecular graphenoids, with carefully designed topological defects have been reported taking advantage of recent advances in on-surface synthesis and scanning probe techniques.<sup>15-25</sup> On-surface synthetic approach involves precursor synthesis in solution and subsequent surface-assisted reactions of precursor building blocks, which permits the synthesized graphene nanostructures with atomic precision and wide tenability.<sup>26-32</sup> After synthesis, the structural and electronic properties of molecular graphenoids can be directly characterized using surface techniques, mainly combined non-contact atomic force microscopy (nc-AFM) and scanning tunneling microscopy (STM) system with single-chemical-bond spatial resolution.<sup>33</sup> Recent studies using bottom-up surface techniques revealed that graphene nanostructures with topological defects host interesting localized electronic states, tunable band gap, and magnetic properties.<sup>21,22,34,35</sup> Compared to the planar configuration of polyaromatic hydrocarbons with purely hexagonal rings, molecular graphenoids with topological defects usually feature a structural curvature.<sup>15,17,18</sup> Typically, such structural deformation is accompanied by a strong electron coupling underneath metal substrate, hindering the detection of their intrinsic magnetic properties. Thus, the characterization of collective magnetic behaviors

originating from multiple topological defects in molecular graphenoids remains a significant challenge.

Here, we report the study of collective high-spin states of a truxene molecule (10,15-dihydro-5H-diindeno[1,2-a:1',2'-c]fluorene), a heptacyclic polyarene structure containing three pentagons with one  $sp^3$  carbon vertex per pentagon ring.<sup>36</sup> Using atom manipulation, we observed that three hydrogen atoms at the  $sp^3$  carbons were controllably dissociated one by one, transforming the  $sp^3$  carbons into  $sp^2$  carbons. Due to their fully aromatic character, up to three unpaired  $\pi$  electrons were introduced into the aromatic topology, forming a high-spin quartet state, suggested by density functional theory (DFT) calculations. High-resolution nc-AFM imaging revealed that the dehydrogenated truxene molecules (DTs) adopted a curved structure on Au(111), with their pentagons having lower adsorption heights. Due to electronic coupling underneath Au(111), the resulting high-spin states of DTs were quenched on Au(111), revealed by scanning tunneling spectroscopy (STS) measurements. To probe their intrinsic electronic structure, we deposited truxene molecules in-situ on an insulating NaCl/Au(111) substrate and dissociated hydrogens one by one, forming DTs. In sharp contrast with Au(111), singly occupied/unoccupied molecular orbitals (SOMOs/SUMOs) were resolved for the generated DTs on NaCl film, which confirmed the presence of high-spin states. Our results could be further extended to realize one-dimensional ferromagnetic chains and two-dimensional ferromagnetic frameworks.

## Experimental Methods

### STM measurement

Sample preparation and characterization were carried out using a commercial low-temperature Unisoku Joule-Thomson scanning probe microscopy (UNISOKU Co., Ltd., Osaka, Japan) under ultra-high vacuum conditions ( $3 \times 10^{-10}$  mbar). Au(111) single-crystal was cleaned by cycles of argon ion sputtering and subsequently annealed to 800 K to obtain atomically flat terraces. NaCl molecules were thermally deposited at 800 K on the clean Au(111) at room temperature for 2 min. Afterward, the sample was transferred to a cryogenic scanner (Traditional UNISOKU Style, UNISOKU Co., Ltd., Osaka, Japan) at 4.9 K for cooling, then truxene was thermally deposited on the clean Au(111) surface with NaCl islands at 10 K. Carbon monoxide molecules were dosed onto the cold sample at  $\sim 7$  K ( $4 \times 10^{-9}$  mbar, 2 min). To achieve ultra-high spatial resolution, a CO molecule was picked up from the Au surface to the apex of the tungsten tip. A quartz tuning fork with a resonant frequency of 26 KHz was used in nc-AFM measurements using the q-Plus sensor (UNISOKU Co., Ltd., Japan). A lock-in amplifier (589 Hz, 0.1-0.5 mV modulation; Nanonis inner lock-in

amplifier, SPECS Surface Nano Analysis GmbH, Berlin, Germany) was used to acquire dI/dV spectra, obtained at 4.9 K unless otherwise stated.

### Spin-polarized DFT calculations

The ground state structures of gas-phase DTs were optimized by the PBE0-D3 (BJ)<sup>37-39</sup> functional combined with the def2-SVP basis set,<sup>40</sup> which was extended to a def2-TZVP basis set<sup>40</sup> for the single point energy calculation. Molecular orbitals and electron spin densities were analyzed by Multiwfn<sup>41</sup> and Visual Molecular Dynamics (VMD).<sup>42</sup> Images of the structures and isosurfaces were

plotted using the Visualization for Electronic and Structural Analysis (VESTA) software.<sup>43</sup>

## Results and Discussion

According to Lieb's theorem and Ovchinnikov's rule, molecular graphenoids with sublattice imbalance in the bipartite honeycomb lattice host tunable magnetic ground states.<sup>14</sup> The spin quantum number  $S$  of the ground state, given by the equation  $S = (N_A - N_B)/2$ , where  $N_A(N_B)$  is the number of carbon atoms in the A(B) sublattice of the graphene honeycomb lattice. As shown in Figure 1a, the application of Lieb's theorem predicated

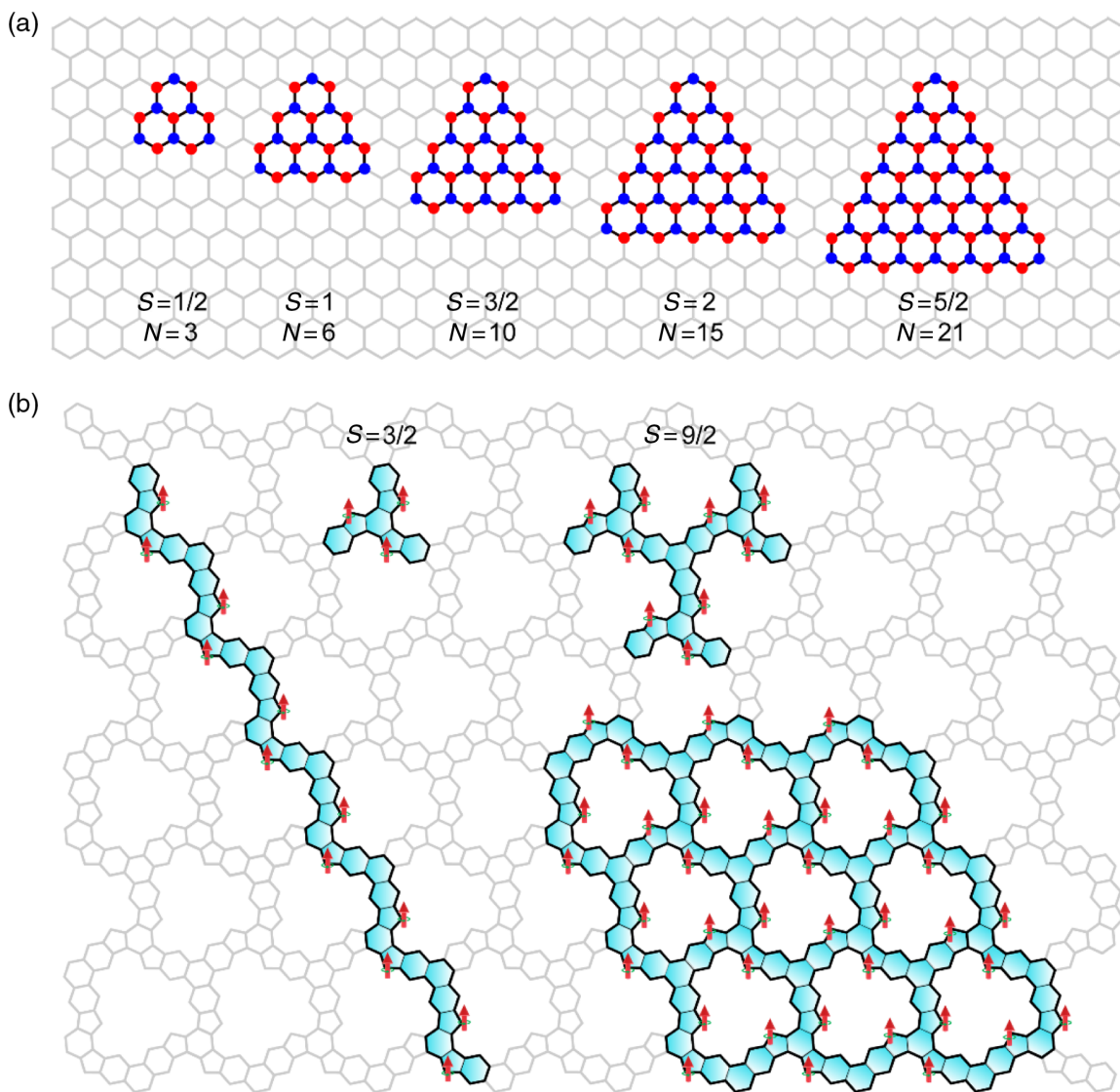


**Figure 1 |** High-spin states in nanographene systems. (a) Magnetic molecules of triangulene-based system with spin  $S$ , while the  $N$  indicates the number of fused benzene rings in triangulene-based molecules. (b) Conceptual routes towards high-spin state molecules, one-dimensional ferromagnetic spin chain, and two-dimensional ferromagnetic network based on truxene.

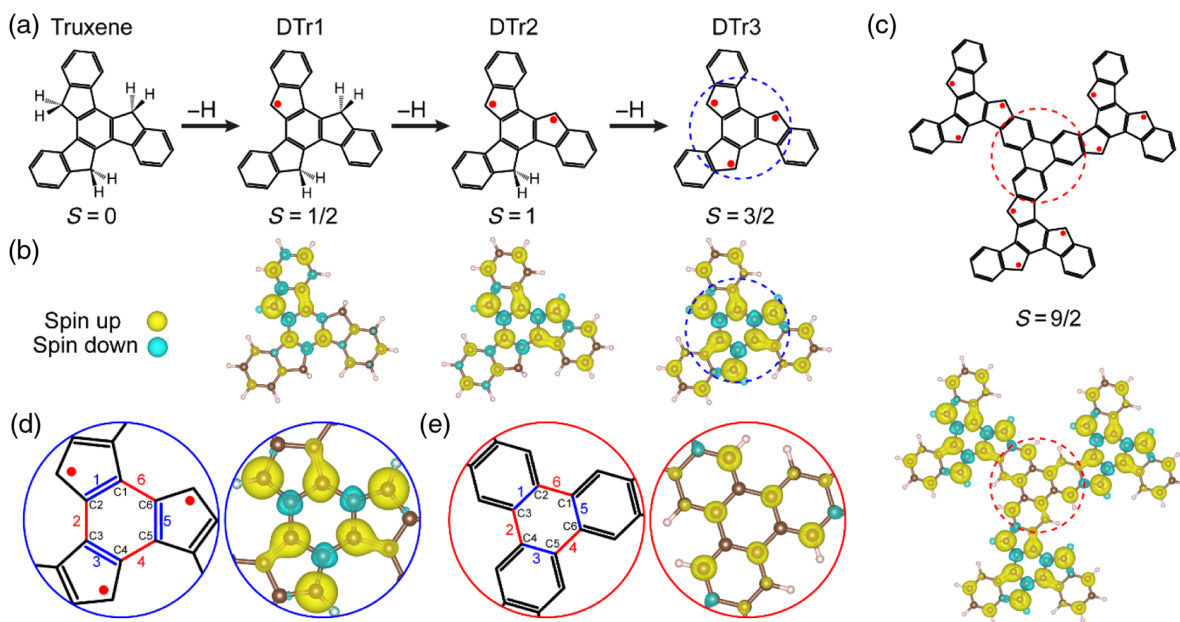


**Figure 2 | Realization of high-spin states in truxene-based frameworks.** (a) Chemical structures of dehydrogenated truxene molecules. (b) Spin-density distributions of DTrs corresponding to (a), respectively. (c) High-spin state of  $S = 9/2$  in a truxene-based trimer. (d) Zoom-in chemical structure and spin density distributions of DTr3 on the center benzene ring marked by a blue dash circle in (a). (e) Zoom-in chemical structure and spin density distributions of DTr3 trimer on the center benzene ring marked by a blue dash circle in (c).

triangular zigzag nanographenes such as triangulene and its larger homologs host tunable magnetic ground states. Experimentally, [2]-triangulene (3 fused rings,  $S = 1/2$ ) and [3]-triangulene (6 fused rings,  $S = 1$ ) have been synthesized in solution, and their open-shell characteristics have been confirmed by electron spin resonance (ESR) spectroscopy<sup>44–47</sup>; [4]-triangulene (10 fused rings,  $S = 3/2$ ), [5]-triangulene (15 fused rings,  $S = 2$ ), and [7]-triangulene (28 fused rings,  $S = 3$ ) have been obtained by on-surface synthesis.<sup>48–51</sup> In the triangulene system, the size of triangulene molecules increased quickly with the spin quantum number  $S$ , where the total required several fused benzene rings in triangulene is given by the equation  $N = (S + 1) \times (2S + 1)$ . Thus, it is challenging to fabricate triangulenes with spin quantum number  $S > 3$  due to difficulties encountered in the synthesis and sublimation of large molecular precursors onto surfaces.

In contrast to sublattice imbalance, the topological defect is much more efficient in introducing unpaired electrons in molecular graphenoids. Incorporating one pentagon ring in molecular graphenoids can introduce one unpaired  $\pi$  electron. In principle, it is possible to build high spin molecules efficiently by periodically positioning electronically coupled topological defects. We performed searches in the molecular database and found that the dehydrogenated truxene molecule (containing three pentagons connected at the 1,3,5-side of the central benzene ring) was an ideal platform to achieve high spin states due

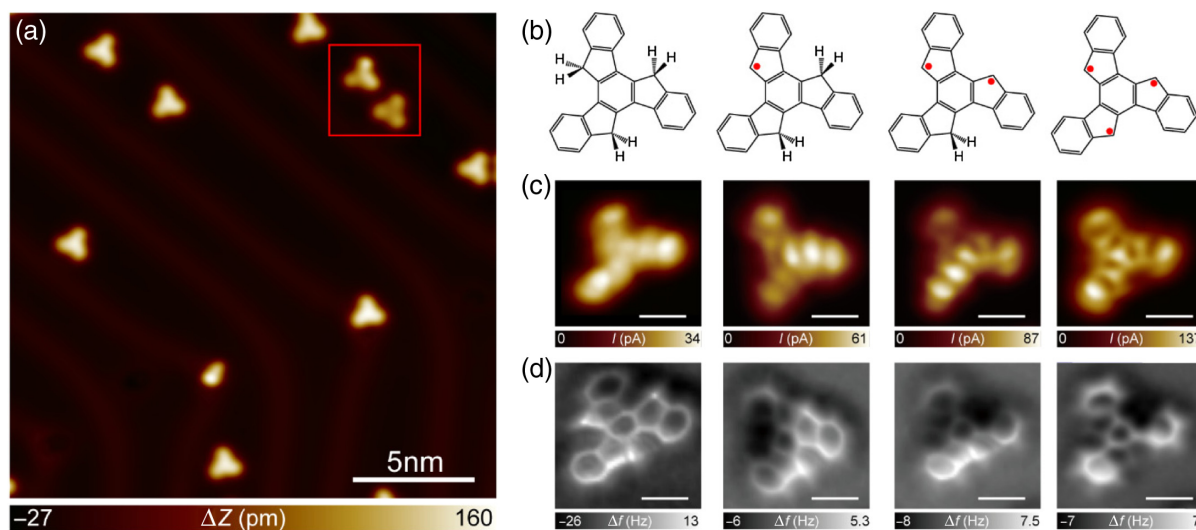
to its C3 symmetry, as confirmed by DFT calculations (Figure 2). More interestingly, extended graphenoids with dehydrogenated truxene building blocks host highly tunable spin states. For example, a molecular graphenoid with three truxene molecular building blocks linked through the 1,3,5-side of a central benzene ring has a ground state spin quantum number of  $S = 9/2$  (Figures 1b and 2c) with only 22 fused rings, which are much less than those required in [10]-triangulene (55 fused rings). Except for designer high spin molecules, the extended one-dimensional dehydrogenated truxene polymer and two-dimensional network would host intriguing one-dimensional ferromagnetism and two-dimensional ferromagnetism with wide tunability for exploring low-dimensional quantum magnetism (Figure 1b). As a first step toward these efforts, we limited our discussion to studying the magnetic ground states of individual truxene building blocks in this work.

Figure 2 depicts the scheme to realize high-spin systems using truxene molecules. Through STM tip-induced atom manipulation or thermal annealing, the hydrogens at the  $sp^3$  carbon sites of truxene molecular precursor could be dissociated one by one, introducing one, two, and three unpaired  $\pi$  electrons inside the molecule, referring to the successive DTrs as DTr1, DTr2, DTr3 for convenience, indicating the presence of one, two, and three unpaired  $\pi$  electrons, respectively (Figure 2a). DFT calculations (Figure 2b) predicated that the unpaired electrons were

ferromagnetically coupled together (the detailed spin density distribution in Figure 2e), forming high-spin triplet and quartet states for the DTr2 and DTr3, respectively. The physics behind such ferromagnetic coupling was attributed to the minimization of on-site Coulomb repulsion in molecular graphenoids with C<sub>3</sub> symmetry.<sup>10</sup> Since the three pentagons were connected to the 1,3,5-side of the central benzene ring; the spin-up density preferred to reside on one sublattice (1,3,5-carbon sites) and the spin-down density on the other sublattice (2,4,6-carbon sites) of the central benzene ring to minimize Coulomb repulsion (the detailed spin density distribution in Figure 2d). In contrast, if the pentagons were connected to the 1,4-side of the central benzene ring, the unpaired electrons would be antiferromagnetically coupled to minimize Coulomb repulsion.<sup>25,52,53</sup> Figure 2c presents the DFT-calculated spin density distribution of a truxene trimer. Owing to its C<sub>3</sub> symmetry, all the unpaired electrons were ferromagnetically coupled together, forming a high spin state with  $S = 9/2$ .

The electronic properties of DTrs on an Au(111) substrate were characterized by high-resolution scanning probe microscopy, as shown in Figure 3. The truxene precursor was synthesized in solution (Supporting Information Figure S1) and thermally deposited on Au(111) (the details in Supporting Information). The sample was then transferred into a low-temperature STM stage holding at 4 K for characterization. A large-scale STM image in Figure 3a revealed a triangular topology of truxene molecules on Au(111). High-resolution nc-AFM imaging resolved the chemical structure of truxene precursor by functionalizing the

tip with a CO molecule, with the sp<sup>3</sup> carbons being imaged as a local bright dot since there is one more hydrogen pointing up from sp<sup>3</sup> carbons (Figure 3d). With tip-induced atom manipulation, one hydrogen at sp<sup>3</sup> carbon was dissociated by positioning the tip above the sp<sup>3</sup> carbon and slowly ramping bias the voltage to 3.2 V (Supporting Information Figure S2). After dehydrogenation, the DTr1 molecule featured a curvature on Au(111), with the dehydrogenated pentagon getting closer to the substrate and the opposite side tilting upward (nc-AFM image in Figure 3d). We further dissociated the other two hydrogens one by one and monitored their structural changes. Similar observations were made on the successive dehydrogenated pentagons, which displayed lower adsorption height than the surrounding benzene rings. As shown in Figure 3c, constant-height current images taken at 3 mV resolved some fine electronic features originating from the highest occupied molecular orbital (HOMO; Supporting Information Figure S3). Scanning tunneling differential conductance spectroscopy was employed in incremental conductance ( $dI/dV$ ) measurements to resolve the detailed electronic properties. For low-energy  $dI/dV$  measurements, no signatures of Kondo resonances were obtained for all DTrs on Au(111) (Supporting Information Figure S4), an effect due to the screening of net spins by conduction electrons of Au(111).<sup>54</sup> The absence of Kondo resonance might be due to either the lack of net spins in the DTrs or Kondo temperature much lower than 4 K. To clarify the physics behind this finding, we performed high energy resolution  $dI/dV$  spectra (Supporting Information Figure S5) and recorded the



**Figure 3 | Structural properties of dehydrogenated truxene molecular graphenoids on Au(111).** (a) Large-scale STM image (bias voltage: 0.5 V, current setpoint: 50 pA; scale bar: 5 nm). Two molecules, as marked by a red square, are dehydrogenated truxenes. (b-d) From top to down: chemical structures, constant-height current images (bias voltage: 3 mV; scale bars: 500 pm), and nc-AFM images (resonant frequency: 26 kHz, oscillation amplitude: 80 pm; scale bars: 500 pm) of truxene precursors, DTr1, DTr2, and DTr3.

DOI: 10.31635/ccschem.022.202201895

Citation: CCS Chem. 2023, 5, 695-703

Link to VoR: <https://doi.org/10.31635/ccschem.022.202201895>

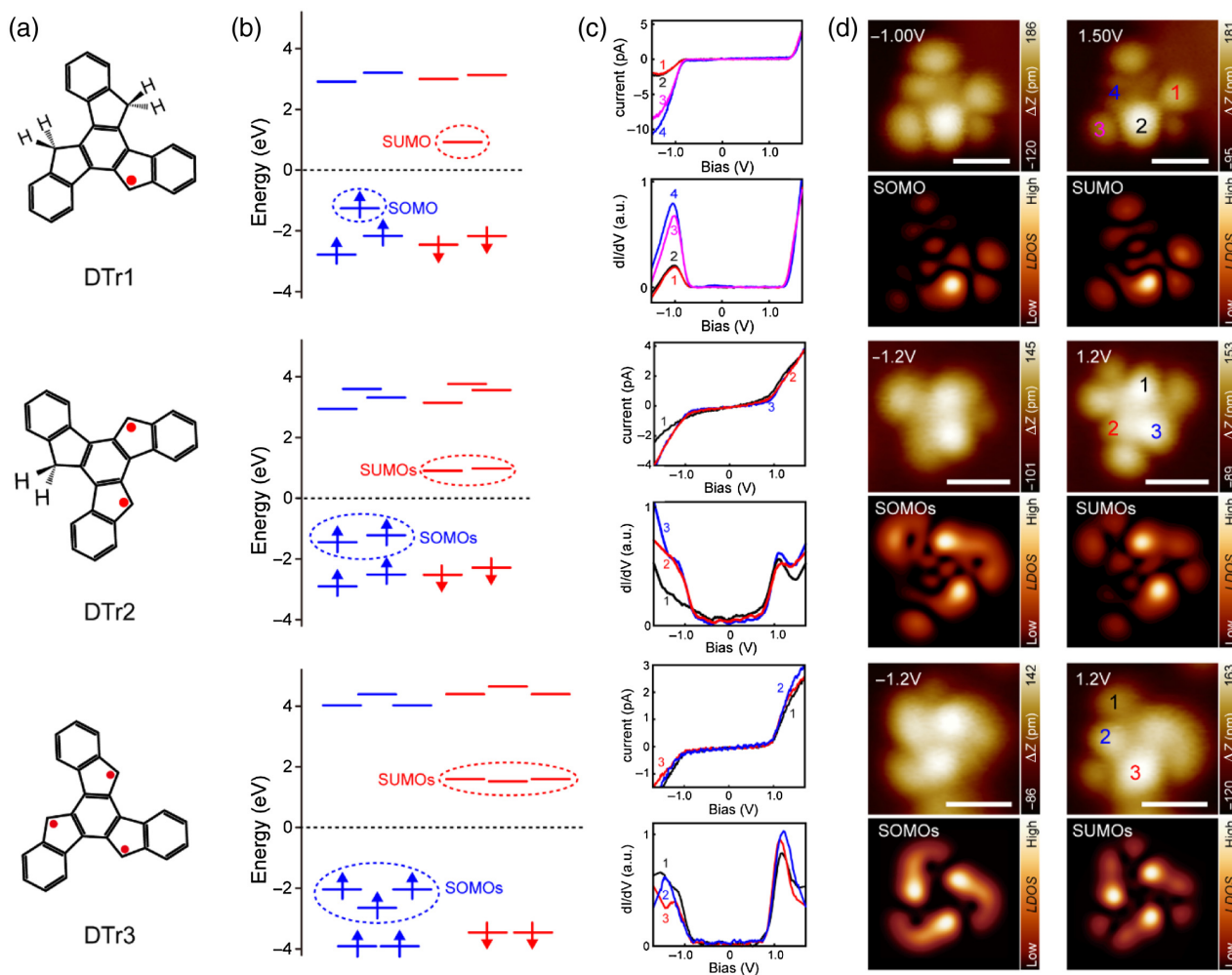


**Figure 4 |** Electronic properties of DTrs on a bilayer NaCl island. (a) Chemical structures of DTr1, DTr2, and DTr3. (b) The corresponding spin-polarized DFT calculated energy spectrum of DTr1, DTr2, and DTr3. (c) I/V spectra and corresponding numerical  $dl/dV$  spectra of DTr1, DTr2, and DTr3, respectively. The positions are marked in (d). (d) Constant current images (current: 3 pA; scale bars: 1 nm) and the corresponding simulated LDOS images of DTr1, DTr2, and DTr3.

corresponding  $dl/dV$  mappings of DTr3. If there indeed exist net spins in DTrs, but with much lower kondo temperature on Au(111), SOMOs resided by the unpaired  $\pi$  electrons should be observed. However, the SOMOs/SUMOs were not detected for DTr3 on Au(111) (Supporting Information Figure S3). Interestingly, all the observed orbitals could be reproduced using molecular orbitals of the undehydrogenated truxene precursor, indicating that the radicals were quenched on Au(111).

To electronically decouple DTrs away from Au(111) metal substrate, we deposited truxene precursors *in situ* on a NaCl/Au(111) substrate held at 8 K. NaCl salts were thermally deposited on Au(111) stored at room temperature, forming self-assembled NaCl monolayer and bilayer islands. The thin NaCl film electronically decoupled single molecules away from the underneath metal substrate efficiently.<sup>47,55</sup> Upon *in situ* deposition, some truxene molecules directly adsorb on the NaCl islands (Supporting

Information Figure S6). Similar to the procedures used for Au(111), we dissociated hydrogens one by one away from the  $sp^3$  carbon sites and monitored their electronic properties. Figure 4 depicts the electronic properties of DTrs on a bilayer NaCl island. DFT-calculated energy spectra indicated that DTr1 hosted a SOMO/SUMO, with a doublet ground state of  $S = 1/2$ . The intrinsic electronic properties of DTr1 on NaCl were observed experimentally. As shown in Figure 4c,  $dl/dV$  spectra taken at different positions of DTr1 resolved the predicted SOMO and SUMO resonances at  $-1$  and  $1.5$  V. STM images in Figure 4d taken at these two energies revealed the orbital shapes of SOMO and SUMO, consistent with STM simulations based on SOMO and SUMO. The presence of SOMO and SUMO confirmed the open-shell electronic structure of DTr1 with a net spin of  $S = 1/2$ . DFT-calculated energy spectra of DTr2 in Figure 4b revealed two SOMOs/SUMOs with a triplet ground state of  $S = 1$ . The orbital shapes of two

SOMOs/SUMOs are shown in Supporting Information Figure S7, with one orbital having quenched density of state at the undehydrogenated corner. Such singly occupied states were confirmed by  $dI/dV$  spectra in Figure 4c, showing two resonance peaks at  $-1$  and  $1$  V, respectively. STM images in Figure 4d taken at these two resonances revealed that the SOMOs and SUMOs have quenched intensity at the undehydrogenated corner, reproduced by the simulated STM images displayed in Figure 4d. Additionally, we excluded the possibility that DTr2 might host a closed-shell electronic structure by comparing its frontier orbitals with the experimental outcomes (Supporting Information Figure S7). The observation of SOMOs and SUMOs, together with their asymmetric spatial distribution, confirmed the triplet high spin state of DTr2 on NaCl. As shown in Figure 4b, fully dehydrogenated DTr3 was predicted to host three SOMOs/SUMOs with a high-spin quartet state. Unlike DTr1 and DTr2, all the SOMOs and SUMOs had delocalized density of states over the entire molecule (Supporting Information Figure S8). As shown in Figure 4c,  $dI/dV$  measurements revealed the presence of SOMOs and SUMOs near  $-1$  and  $1$  V. A threefold symmetric spatial distribution of SOMOs and SUMOs was confirmed by STM imaging in Figure 4d, in agreement with STM simulations. Additionally, we excluded the possibility of DTr3 with a ground state of  $S = 1/2$  by comparing its frontier orbitals with experiments (Supporting Information Figure S8). The resolved intrinsic electronic properties of DTr2 and DTr3 on NaCl suggested the presence of collective high-spin triplet and quartet states in truxene-based molecular graphenoids with two and three pentagon defects, respectively.

## Conclusion

We have demonstrated the realization of collective high spin states in molecular graphenoids with regular organized topological defects. By combining DFT calculations with scanning probe measurements, the presence of collective high spin states of DTrs on a thin insulating film was confirmed by resolving the SOMOs/SUMOs. Our research not only paves the way for engineering collective high spin states induced by topological defects but also provides a new platform for efficient fabrication of ferromagnetic frameworks such as one-dimensional spin chains and two-dimensional networks with implications for exploring quantum magnetism, as well as quantum technological implications.

We would also like to note that similar work was published recently by Mishra et al.<sup>56</sup>

## Supporting Information

Supporting Information is available and includes detailed experimental methods and computational details.

DOI: 10.31635/ccschem.022.202201895

Citation: CCS Chem. 2023, 5, 695–703

Link to VoR: <https://doi.org/10.31635/ccschem.022.202201895>

## Competing Interests

The authors declare no competing financial interests.

## Preprint Statement

The research presented in this article was posted on a preprint server before publication in CCS Chemistry. The corresponding preprint article can be found here: <https://arxiv.org/abs/2202.03853>

## Acknowledgments

S.W. acknowledges the financial support from the National Key R&D Program of China (grant no. 2020YFA0309000), the National Natural Science Foundation of China (grant nos. 11874258 and 12074247), the Shanghai Municipal Science and Technology Qi Ming Xing Project (grant no. 20QA1405100), Fok Ying Tung Foundation for young researchers and SJTU (grant no. 21XO10200846). This work is also supported by the Ministry of Science and Technology of China (grant nos. 2019YFA0308600, 2016YFA0301003, and 2016YFA0300403), NSFC (grants nos. 21925201, 11521404, 11634009, 92065201, 11874256, 11790313, and 11861161003), the Strategic Priority Research Program of Chinese Academy of Sciences (grant no. XDB28000000), and the Science and Technology Commission of Shanghai Municipality (grants nos. 20ZR1414200, 2019SHZDZX01, 19JC1412701, and 20QA1405100) for partial support.

## References

1. Fan, Q.; Yan, L.; Tripp, M. W.; Krejčí, O.; Dimosthenous, S.; Kachel, S. R.; Chen, M.; Foster, A. S.; Koert, U.; Liljeroth, P.; Gottfried, J. M. Biphenylene Network: A Nonbenzenoid Carbon Allotrope. *Science* **2021**, *372*, 852–856.
2. Lombardi, F.; Lodi, A.; Ma, J.; Liu, J.; Slota, M.; Narita, A.; Myers, W. K.; Müllen, K.; Feng, X.; Bogani, L. Quantum Units from the Topological Engineering of Molecular Graphenoids. *Science* **2019**, *366*, 1107–1110.
3. Liu, M.; Liu, M.; She, L.; Zha, Z.; Pan, J.; Li, S.; Li, T.; He, Y.; Cai, Z.; Wang, J.; Zheng, Y.; Qiu, X.; Zhong, D. Graphene-Like Nanoribbons Periodically Embedded with Four- and Eight-Membered Rings. *Nat. Commun.* **2017**, *8*, 14924.
4. Zhang, Y.; Li, S.-Y.; Huang, H.; Li, W.-T.; Qiao, J.-B.; Wang, W.-X.; Yin, L.-J.; Bai, K.-K.; Duan, W.; He, L. Scanning Tunneling Microscopy of the  $\pi$  Magnetism of a Single Carbon Vacancy in Graphene. *Phys. Rev. Lett.* **2016**, *117*, 166801.
5. Gonzalez-Herrero, H.; Gomez-Rodriguez, J. M.; Mallet, P.; Moaied, M.; Palacios, J. J.; Salgado, C.; Ugeda, M. M.; Veuillen, J.-Y.; Yndurain, F.; Brihuega, I. Atomic-Scale Control of Graphene Magnetism by Using Hydrogen Atoms. *Science* **2016**, *352*, 437–441.
6. Cui, P.; Zhang, Q.; Zhu, H.; Li, X.; Wang, W.; Li, Q.; Zeng, C.; Zhang, Z. Carbon Tetragons as Definitive Spin Switches in

- Narrow Zigzag Graphene Nanoribbons. *Phys. Rev. Lett.* **2016**, *116*, 026802.
7. Nair, R. R.; Sepioni, M.; Tsai, I.-L.; Lehtinen, O.; Keinonen, J.; Krasheninnikov, A. V.; Thomson, T.; Geim, A. K.; Grigorieva, I. V. Spin-Half Paramagnetism in Graphene Induced by Point Defects. *Nat. Phys.* **2012**, *8*, 199.
8. Alexandre, S. S.; Lúcio, A. D.; Neto, A. H. C.; Nunes, R. W. Correlated Magnetic States in Extended One-Dimensional Defects in Graphene. *Nano Lett.* **2012**, *12*, 5097–5102.
9. Sun, Z.; Wu, J. Open-Shell Polycyclic Aromatic Hydrocarbons. *J. Mater. Chem.* **2012**, *22*, 4151–4160.
10. Yazyev, O. V. Emergence of Magnetism in Graphene Materials and Nanostructures. *Rep. Prog. Phys.* **2010**, *73*, 056501.
11. Červenka, J.; Katsnelson, M. I.; Flipse, C. F. J. Room-Temperature Ferromagnetism in Graphite Driven by Two-Dimensional Networks of Point Defects. *Nat. Phys.* **2009**, *5*, 840–844.
12. Palacios, J. J.; Fernández-Rossier, J.; Brey, L. Vacancy-Induced Magnetism in Graphene and Graphene Ribbons. *Phys. Rev. B* **2008**, *77*, 195428.
13. Yazyev, O. V.; Helm, L. Defect-Induced Magnetism in Graphene. *Phys. Rev. B* **2007**, *75*, 125408.
14. Lieb, E. H. Two Theorems on the Hubbard Model. *Phys. Rev. Lett.* **1989**, *62*, 1201–1204.
15. Chaolumen, Stepek, I. A.; Yamada, K. E.; Ito, H.; Itami, K. Construction of Heptagon-Containing Molecular Nanocarbons. *Angew. Chem. Int. Ed.* **2021**, *60*, 23508–23532.
16. Li, L.; Mahapatra, S.; Liu, D.; Lu, Z.; Jiang, N. On-Surface Synthesis and Molecular Engineering of Carbon-Based Nanoarchitectures. *ACS Nano* **2021**, *15*, 3578–3585.
17. Mallada, B.; de la Torre, B.; Mendieta-Moreno, J. I.; Nachtigallová, D.; Matěj, A.; Matoušek, M.; Mutombo, P.; Brabec, J.; Veis, L.; Cadart, T.; Kotora, M.; Jelínek, P. On-Surface Strain-Driven Synthesis of Nonalternant Non-Benzoid Aromatic Compounds Containing Four- to Eight-Membered Rings. *J. Am. Chem. Soc.* **2021**, *143*, 14694–14702.
18. Hou, I. C.-Y.; Sun, Q.; Eimre, K.; Di Giovannantonio, M.; Urgel, J. I.; Ruffieux, P.; Narita, A.; Fasel, R.; Müllen, K. On-Surface Synthesis of Unsaturated Carbon Nanostructures with Regularly Fused Pentagon-Heptagon Pairs. *J. Am. Chem. Soc.* **2020**, *142*, 10291–10296.
19. Urgel, J. I.; Di Giovannantonio, M.; Eimre, K.; Lohr, T. G.; Liu, J.; Mishra, S.; Sun, Q.; Kinikar, A.; Widmer, R.; Stoltz, S.; Bommert, M.; Berger, R.; Ruffieux, P.; Pignedoli, C. A.; Müllen, K.; Feng, X.; Fasel, R. On-Surface Synthesis of Cumulene-Containing Polymers via Two-Step Dehalogenative Homocoupling of Dibromomethylene-Functionalized Tribenzoazulene. *Angew. Chem. Int. Ed.* **2020**, *132*, 13383–13389.
20. Wäckerlin, C.; Gallardo, A.; Mairena, A.; Baljozović, M.; Cahlik, A.; Antalík, A.; Brabec, J.; Veis, L.; Nachtigallová, D.; Jelínek, P.; Ernst, K.-H. On-Surface Hydrogenation of Buckybowls: From Curved Aromatic Molecules to Planar Non-Kekulé Aromatic Hydrocarbons. *ACS Nano* **2020**, *14*, 16735–16742.
21. Mishra, S.; Beyer, D.; Berger, R.; Liu, J.; Gröning, O.; Urgel, J. I.; Müllen, K.; Ruffieux, P.; Feng, X.; Fasel, R. Topological Defect-Induced Magnetism in a Nanographene. *J. Am. Chem. Soc.* **2020**, *142*, 1147–1152.
22. Li, J.; Sanz, S.; Corso, M.; Choi, D. J.; Peña, D.; Frederiksen, T.; Pascual, J. I. Single Spin Localization and Manipulation in Graphene Open-Shell Nanostructures. *Nat. Commun.* **2019**, *10*, 200.
23. Skidin, D.; Eisenhut, F.; Richter, M.; Nikipar, S.; Krüger, J.; Ryndyk, D. A.; Berger, R.; Cuniberti, G.; Feng, X.; Moresco, F. On-Surface Synthesis of Nitrogen-Doped Nanographenes with 5–7 Membered Rings. *Chem. Commun.* **2019**, *55*, 4731–4734.
24. Mishra, S.; Lohr, T. G.; Pignedoli, C. A.; Liu, J.; Berger, R.; Urgel, J. I.; Müllen, K.; Feng, X.; Ruffieux, P.; Fasel, R. Tailoring Bond Topologies in Open-Shell Graphene Nanostructures. *ACS Nano* **2018**, *12*, 11917–11927.
25. Majzik, Z.; Pavláček, N.; Vilas-Varela, M.; Pérez, D.; Moll, N.; Guitián, E.; Meyer, G.; Peña, D.; Gross, L. Studying an Antiaromatic Polycyclic Hydrocarbon Adsorbed on Different Surfaces. *Nat. Commun.* **2018**, *9*, 1198.
26. Grill, L.; Dyer, M.; Lafferentz, L.; Persson, M.; Peters, M. V.; Hecht, S. Nano-Architectures by Covalent Assembly of Molecular Building Blocks. *Nat. Nanotechnol.* **2007**, *2*, 687–691.
27. Grill, L.; Hecht, S. Covalent On-Surface Polymerization. *Nat. Chem.* **2020**, *12*, 115–130.
28. Cai, J.; Ruffieux, P.; Jaafar, R.; Bieri, M.; Braun, T.; Blanckenburg, S.; Muoth, M.; Seitsonen, A. P.; Saleh, M.; Feng, X.; Müllen, K.; Fasel, R. Atomically Precise Bottom-Up Fabrication of Graphene Nanoribbons. *Nature* **2010**, *466*, 470–473.
29. Yuan, B.; Li, C.; Zhao, Y.; Gröning, O.; Zhou, X.; Zhang, P.; Guan, D.; Li, Y.; Zheng, H.; Liu, C.; Mai, Y.; Liu, P.; Ji, W.; Jia, J.; Wang, S. Resolving Quinoid Structure in Poly(Para-Phenylenes) Chains. *J. Am. Chem. Soc.* **2020**, *142*, 10034–10041.
30. Clair, S.; de Oteyza, D. G. Controlling a Chemical Coupling Reaction on a Surface: Tools and Strategies for On-Surface Synthesis. *Chem. Rev.* **2019**, *119*, 4717–4776.
31. Albrecht, F.; Rey, D.; Fatayer, S.; Schulz, F.; Pérez, D.; Peña, D.; Gross, L. Intramolecular Coupling of Terminal Alkynes by Atom Manipulation. *Angew. Chem. Int. Ed.* **2020**, *59*, 22989–22993.
32. Li, X.; Niu, K.; Zhang, J.; Yu, X.; Zhang, H.; Wang, Y.; Guo, Q.; Wang, P.; Li, F.; Hao, Z.; Xu, C.; Tang, Y.; Xu, Z.; Lu, S.; Liu, P.; Xue, G.; Wei, Y.; Chi, L. Direct Transformation of N-Alkane into All-Trans Conjugated Polyene via Cascade Dehydrogenation. *Natl. Sci. Rev.* **2021**, *8*, nwab093.
33. Gross, L.; Mohn, F.; Moll, N.; Liljeroth, P.; Meyer, G. The Chemical Structure of a Molecule Resolved by Atomic Force Microscopy. *Science* **2009**, *325*, 1110–1114.
34. Zheng, Y.; Li, C.; Zhao, Y.; Beyer, D.; Wang, G.; Xu, C.; Yue, X.; Chen, Y.; Guan, D.-D.; Li, Y.-Y.; Zheng, H.; Liu, C.; Luo, W.; Feng, X.; Wang, S.; Jia, J. Engineering of Magnetic Coupling in Nanographene. *Phys. Rev. Lett.* **2020**, *124*, 147206.
35. Zheng, Y.; Li, C.; Xu, C.; Beyer, D.; Yue, X.; Zhao, Y.; Wang, G.; Guan, D.; Li, Y.; Zheng, H.; Liu, C.; Liu, J.; Wang, X.; Luo, W.; Feng, X.; Wang, S.; Jia, J. Designer Spin Order in Diradical Nanographenes. *Nat. Commun.* **2020**, *11*, 6076.
36. Goubard, F.; Dumur, F. Truxene: A Promising Scaffold for Future Materials. *RSC Adv.* **2015**, *5*, 3521–3551.

37. Adamo, C.; Barone, V. Toward Reliable Density Functional Methods without Adjustable Parameters: The PBE0 Model. *J. Chem. Phys.* **1999**, *110*, 6158–6170.
38. Grimme, S.; Antony, J.; Ehrlich, S.; Krieg, H. A Consistent and Accurate *Ab Initio* Parametrization of Density Functional Dispersion Correction (DFT-D) for the 94 Elements H-Pu. *J. Chem. Phys.* **2010**, *132*, 154104.
39. Grimme, S.; Ehrlich, S.; Goerigk, L. Effect of the Damping Function in Dispersion Corrected Density Functional Theory. *J. Comput. Chem.* **2011**, *32*, 1456–1465.
40. Weigend, F.; Ahlrichs, R. Balanced Basis Sets of Split Valence, Triple Zeta Valence and Quadruple Zeta Valence Quality for H to Rn: Design and Assessment of Accuracy. *Phys. Chem. Chem. Phys.* **2005**, *7*, 3297–3305.
41. Lu, T.; Chen, F. Multiwfn: A Multifunctional Wavefunction Analyzer. *J. Comput. Chem.* **2021**, *33*, 580–592.
42. Humphrey, W.; Dalke, A.; Schulten, K. VMD: Visual Molecular Dynamics. *J. Mol. Graph.* **1996**, *14*, 33–38.
43. Momma, K.; Izumi, F. VESTA 3 for Three-Dimensional Visualization of Crystal, Volumetric and Morphology Data. *J. App. Crystall.* **2011**, *44*, 1272–1276.
44. Inoue, J.; Fukui, K.; Kubo, T.; Nakazawa, S.; Sato, K.; Shiomi, D.; Morita, Y.; Yamamoto, K.; Takui, T.; Nakasuji, K. The First Detection of a Clar's Hydrocarbon, 2,6,10-Tri-Tert-Butyltriangulene: A Ground-State Triplet of Non-Kekulé Polynuclear Benzenoid Hydrocarbon. *J. Am. Chem. Soc.* **2001**, *123*, 12702–12703.
45. Goto, K.; Kubo, T.; Yamamoto, K.; Nakasuji, K.; Sato, K.; Shiomi, D.; Takui, T.; Kubota, M.; Kobayashi, T.; Yakusi, K.; Ouyang, J. A Stable Neutral Hydrocarbon Radical: Synthesis, Crystal Structure, and Physical Properties of 2,5,8-Tri-Tert-Butyl-Phenalenyl. *J. Am. Chem. Soc.* **1999**, *121*, 1619–1620.
46. Allinson, G.; Bushby, R. J.; Paillaud, J. L.; Oduwole, D.; Sales, K. ESR Spectrum of a Stable Triplet Pi. Biradical: Trioxytriangulene. *J. Am. Chem. Soc.* **1993**, *115*, 2062–2064.
47. Pavliček, N.; Mistry, A.; Majzik, Z.; Moll, N.; Meyer, G.; Fox, D. J.; Gross, L. Synthesis and Characterization of Triangulene. *Nat. Nanotechnol.* **2017**, *12*, 308–311.
48. Su, J.; Telychko, M.; Hu, P.; Macam, G.; Mutombo, P.; Zhang, H.; Bao, Y.; Cheng, F.; Huang, Z.-Q.; Qiu, Z.; Tan, S. J. R.; Lin, H.; Jelínek, P.; Chuang, F.-C.; Wu, J.; Lu, J. Atomically Precise Bottom-up Synthesis of  $\pi$ -Extended [5]Triangulene. *Sci. Adv.* **2019**, *5*, eaav7717.
49. Mishra, S.; Beyer, D.; Eimre, K.; Liu, J.; Berger, R.; Gröning, O.; Pignedoli, C. A.; Müllen, K.; Fasel, R.; Feng, X.; Ruffieux, P. Synthesis and Characterization of  $\pi$ -Extended Triangulene. *J. Am. Chem. Soc.* **2019**, *141*, 10621–10625.
50. Su, J.; Fan, W.; Mutombo, P.; Peng, X.; Song, S.; Ondráček, M.; Golub, P.; Brabec, J.; Veis, L.; Telychko, M.; Jelínek, P.; Wu, J.; Lu, J. On-Surface Synthesis and Characterization of [7]Triangulene Quantum Ring. *Nano Lett.* **2021**, *21*, 861–8677.
51. Mishra, S.; Xu, K.; Eimre, K.; Komber, H.; Ma, J.; Pignedoli, C. A.; Fasel, R.; Feng, X.; Ruffieux, P. Synthesis and Characterization of [7]Triangulene. *Nanoscale* **2021**, *13*, 1624–1628.
52. Shimizu, A.; Kishi, R.; Nakano, M.; Shiomi, D.; Sato, K.; Takui, T.; Hisaki, I.; Miyata, M.; Tobe, Y. Indeno[2,1-b]Fluorene: A 20- $\pi$ -Electron Hydrocarbon with Very Low-Energy Light Absorption. *Angew. Chem. Int. Ed.* **2013**, *52*, 6076–6079.
53. Di Giovannantonio, M.; Eimre, K.; Yakutovich, A. V.; Chen, Q.; Mishra, S.; Urgel, J. I.; Pignedoli, C. A.; Ruffieux, P.; Müllen, K.; Narita, A.; Fasel, R. On-Surface Synthesis of Antiaromatic and Open-Shell Indeno[2,1-b]Fluorene Polymers and Their Lateral Fusion into Porous Ribbons. *J. Am. Chem. Soc.* **2019**, *141*, 12346–12354.
54. Ternes, M.; Heinrich, A. J.; Schneider, W.-D. Spectroscopic Manifestations of the Kondo Effect on Single Adatoms. *J. Phys. Condens. Matter* **2009**, *21*, 053001.
55. Wang, S.; Talirz, L.; Pignedoli, C. A.; Feng, X.; Müllen, K.; Fasel, R.; Ruffieux, P. Giant Edge State Splitting at Atomically Precise Graphene Zigzag Edges. *Nat. Commun.* **2016**, *7*, 11507.
56. Mishra, S.; Fatayer, S.; Fernández, S.; Kaiser, K.; Peña, D.; Gross, L. Nonbenzenoid High-Spin Polycyclic Hydrocarbons Generated by Atom Manipulation. *ACS Nano* **2022**, *16*, 3264–3271.